Metallic-covalent interatomic potential for carbon in iron

Derek J. Hepburn* and Graeme J. Ackland†
School of Physics, CSEC and SUPA, The University of Edinburgh, Mayfield Road, Edinburgh EH9 3JZ, United Kingdom
(Received 22 September 2008; published 15 October 2008)

Existing interatomic potentials for the iron-carbon system suffer from qualitative flaws in describing even the simplest of defects. In contrast to more accurate first-principles calculations, all previous potentials show strong bonding of carbon to overcoordinated defects (e.g., self-interstitials, dislocation cores) and a failure to accurately reproduce the energetics of carbon-vacancy complexes. Thus any results from their application in molecular dynamics to more complex environments are unreliable. The problem arises from a fundamental error in potential design—the failure to describe short-ranged covalent bonding of the carbon *p* electrons. We describe a resolution to the problem and present an empirical potential based on insights from density-functional theory, showing covalent-type bonding for carbon. The potential correctly describes the interaction of carbon and iron across a wide range of defect environments. It has the embedded atom method form and hence appropriate for billion atom molecular-dynamics simulations.

DOI: 10.1103/PhysRevB.78.165115 PACS number(s): 61.50.Ah, 31.15.xv, 61.72.J−, 61.82.Bg

I. INTRODUCTION

Spanning more than ten orders of magnitude in length and twenty in time, materials modeling is an essentially multiscale challenge. With different physics at each level, practical approaches are hierarchical, with well defined methods such as density-functional theory (DFT), kinetic Monte Carlo (kMC), molecular dynamics (MD), dislocation dynamics, and finite-element modeling all well developed for modeling steels.

These techniques were developed independently and have evolved to a high degree of sophistication. However, each requires extrinsic inputs: correlation functionals, migration energies, interatomic potentials, Peierls stress, Burgers vector, materials properties, etc. Correctly bridging the existing hierarchy is perhaps the most challenging problem facing multiscale modeling. This is most prominent at the interface between DFT and MD, where an interatomic potential is required to capture, in a few parameters, the essential physics described by millions of variables in DFT. Ideally, the interatomic potential should also be compatible with community MD codes.[1–5] Meeting these multiple constraints makes the creation of empirical potentials a challenging and often inelegant task.

Steel is such an important material that it may seem surprising that few good interatomic potentials have been proposed. There are a number of reasons for this. Iron itself is difficult to model due to ferromagnetism and phase transitions at temperature and pressure. These two phenomena are intimately entangled, the ambient bcc α phase is stabilized by its ferromagnetism, the high-pressure hcp ϵ phase is nonmagnetic, and a proper description of the high-T fcc γ phase should include paramagnetism. Including explicit magnetic degrees of freedom is possible but undesirable: it increases complexity and would be incompatible with current MD codes. Consequently, previous iron potentials have confined themselves to a single phase, typically α,[6–9] modeled using the embedded atom method[10] (EAM) or a computationally equivalent scheme.[11–15] Here the energy is a species-dependent function of a sum of pairwise interactions. This idea dates back to the second-moment approximation to tight binding,[11,16,17] which gives clear indication of the systems and properties where it is appropriate (primarily, close-packed transition metals). The absence of explicit magnetism in such models has been justified by recent work showing that a treatment of ferromagnetism in the two-band second-moment tight-binding approximation gives EAM-equivalent potentials[12,18,19] but not the essential physics determining crystal structure, i.e., the shape of the bands.[20]

Carbon is also problematic; neither the graphite nor diamond phase is close packed but can be modeled within EAM by ensuring that the chosen equilibrium structure is energetically saturated by four near neighbors.[13–15] In iron, carbon adopts an off-lattice position—the octahedral (O) site—which has much lower energy than the tetrahedral (T) site. Carbon atoms do not bond covalently to one another in the matrix, preferring to bond directly with iron, but exhibit covalent-type bonding in vacancies.[21]

A further reason for the lack of progress is that pair potentials by Johnson,[22] both for pure iron and carbon in iron, were in accord with the known experimental data in the 1960's. Recently, however, *ab initio* data has extended the number of configurations for which energies are reliably known and better parametrizations for pure iron have become available.[6,7] Such calculations in iron-carbon[21–26] have exposed two major failings of existing potentials.

Firstly, the carbon solvation energy (i.e., the energy released when free carbon enters solid solution) is large at around 6 eV. In contrast to carbon, the nitrogen solvation energy is approximately 5 eV lower.[21] DFT shows that three *p*-type electronic states of both carbon and nitrogen lie well below the Fermi energy of iron.[21] For nitrogen these states are filled by three atomic *p* electrons whereas for carbon one state remains unfilled. Donation from the iron *d* band to fill this state provides an intuitive mechanism for the additional solvation energy seen for carbon. This electron transfer occurs whenever carbon atoms come close to solid.

The second main failing of existing iron-carbon potentials is the absence of covalent bonding. *Ab initio* charge-density data[21] shows that octahedrally sited carbon forms *p*-type covalent bonds to its *two* near neighbors with a bond length of

1.77 Å, and no significant bonding to second neighbors. A tetrahedrally sited carbon shows no such bond formation. In contrast, existing potentials stabilize the octahedral site over the tetrahedral by having *six* iron-carbon bonds rather than four. A consequence of this incorrect heuristic is that carbon is also attracted to high-coordination defects, in conflict with the repulsion seen between carbon and self-interstitial defects in *ab initio* calculations.

Ab initio calculations have also provided evidence for covalent bonding between carbon atoms in vacancy-type defects.[21,24,26] In particular Domain *et al.*[21] show that two carbons in a vacancy form a dimer with a short bond length of 1.42 Å, an additional binding of 0.56 eV (Ref. 21) above that for two carbon atoms in separate vacancies and a build up of charge density between the two carbons, all consistent with covalent bond formation.

In this work we present a resolution to these problems by incorporating the effects of solvation and covalent bonding within the EAM framework. We first present and motivate the functional forms we have used to model the iron-carbon system, then discuss our fitting strategy, and finally compare the performance of our potential with that of existing potentials and with *ab initio* calculations.

II. INTERATOMIC IRON-CARBON POTENTIAL

The most general form for the energy, U, for EAM-type potentials is given by

$$U(\{r_{ab}\}) = \sum_{a,b>a} V^{(X_a,X_b)}(r_{ab}) + \sum_a F^{(X_a)}(\rho_a), \tag{1}$$

$$\rho_a = \sum_{b\neq a} \phi^{(X_a,X_b)}(r_{ab}), \tag{2}$$

where $V^{(X_a,X_b)}$, $\phi^{(X_a,X_b)}$, and $F^{(X_a)}$ are parametrized functions dependent on element types, X_a and X_b. $F^{(X_a)}$ represents the local band-structure energy of atom a of type X_a. It is worth noting that the cross-species pair potentials are assumed identical here, i.e., $V^{(X,Y)} \equiv V^{(Y,X)}$ when $X \neq Y$, but the cross-species ϕ functions are not equivalent in general.

In this work we confine our potential to describing the ferromagnetic bcc α phase, taking our iron interactions, i.e., $V^{(\mathrm{Fe,Fe})}(r)$, $\phi^{(\mathrm{Fe,Fe})}(r)$, and $F^{(\mathrm{Fe})}(\rho)$, from a recent potential fitted to a wide range of defect configurations.[6] For steels the elemental environment of carbon is irrelevant so we have not attempted to model pure carbon here. Instead we concentrate on modeling carbon-iron and carbon-carbon interactions within iron.

For the iron-carbon and carbon-carbon pair potentials, we take the universal screened electrostatic potential of Biersack and Ziegler[27] at short range connected to an empirically fitted spline function with cutoff. The spline function is determined by specifying a set of function values, $\{f_i, i \in [1,n-1]\}$, at a set of spline points, $\{s_i, i \in [1,n-1]\}$. Continuity of the function between these points is ensured down to the second derivative level using polynomial interpolation functions, $V_i^{(X,\mathrm{C})}(r)$, with coefficients determined appropriately. We use quartic polynomials for $V_0^{(X,\mathrm{C})}$ and $V_{n-1}^{(X,\mathrm{C})}$, and cubic polynomials otherwise. In detail,

$$V^{(X,\mathrm{C})}(r) = \begin{cases} \dfrac{Z_X Z_C e^2}{4\pi\epsilon_0 r}\xi(r/r_s) & r \leq s_0 \\ V_i^{(X,\mathrm{C})}(r) & s_i < r < s_{i+1},\ i \in [0,n-1] \\ f_i & r = s_i,\ i \in [1,n-1] \\ 0 & r \geq s_n = r_c \end{cases}, \tag{3}$$

where X can be either Fe or C, Z_X and Z_C are the atomic numbers of species X and carbon, respectively, $r_s = 0.88534 a_b / \sqrt{Z_X^{2/3} + Z_C^{2/3}}$, a_b is the Bohr radius, and

$$\xi(x) = 0.1818e^{-3.2x} + 0.5099e^{-0.9423x} + 0.2802e^{-0.4029x} + 0.02817e^{-0.2016x}. \tag{4}$$

For notational simplicity the radius at which the spline joins the Biersack-Ziegler part is specified as s_0 and the cut-off radius, r_c, specified as s_n. The spline points, $\{s_i, i \in [0,n]\}$, and the function values, $\{f_i, i \in [1,n-1]\}$, are taken as the adjustable parameters for the purposes of fitting.

We have modeled the large solvation energy of carbon in iron and the associated electron transfer by requiring that the carbon embedding function, $F^{(\mathrm{C})}$, takes a value appropriate for solvation whenever $\phi^{(\mathrm{C,Fe})}$ registers the presence of iron. We also assign the energy from carbon covalent bonding to $F^{(\mathrm{C})}$, which band structure suggests is due to the carbon p orbitals.[21]

The actual functional form for the carbon embedding function is given by

$$F^{(\mathrm{C})}(\rho) = \begin{cases} 0 & \rho \leq 0 \\ F_1^{(\mathrm{C})}(\rho) & 0 < \rho \leq \rho_1 \\ E_{\mathrm{sol}} & \rho_1 < \rho \leq \rho_2 \\ F_2^{(\mathrm{C})}(\rho) & \rho_2 < \rho \leq 2\rho_2 \\ E_{\mathrm{sol}} + E_{\mathrm{bond}} & \rho > 2\rho_2 \end{cases}, \tag{5}$$

where the cubic interpolating polynomials, $F_i^{(\mathrm{C})}$, ensure continuity of the function and its derivative. Carbon can be said to be in solution for $\rho \geq \rho_1$, where we fix $\rho_1 = 0.001$, and the covalent bonding initiated for $\rho \geq \rho_2 = 0.5$, becoming fully formed only when $\rho \geq 2\rho_2 = 1$. The two energies, E_{sol} and E_{bond}, which determine how much energy is gained by carbon upon entering solution and upon forming covalent bonds, respectively, are the only fitting parameters from this function.

The function, $\phi^{(\mathrm{C,Fe})}(r)$, had the following complementary form for the description of solvation and carbon-iron covalent bonding,

$$\phi^{(\mathrm{C,Fe})}(r) = \begin{cases} \rho_2 & r \leq r_1 \\ \phi_1^{(\mathrm{C,Fe})}(r) & r_1 < r \leq r_2 \\ \rho_1 & r_2 < r \leq r_3 \\ \phi_2^{(\mathrm{C,Fe})}(r) & r_3 < r \leq r_4 \\ 0 & r > r_4 \end{cases}, \tag{6}$$

where the cubic interpolating polynomials, $\phi_i^{(\mathrm{C,Fe})}$, ensure continuity of the function and its derivative between the plateau regions. The radii, r_3 and r_4, set the range over which

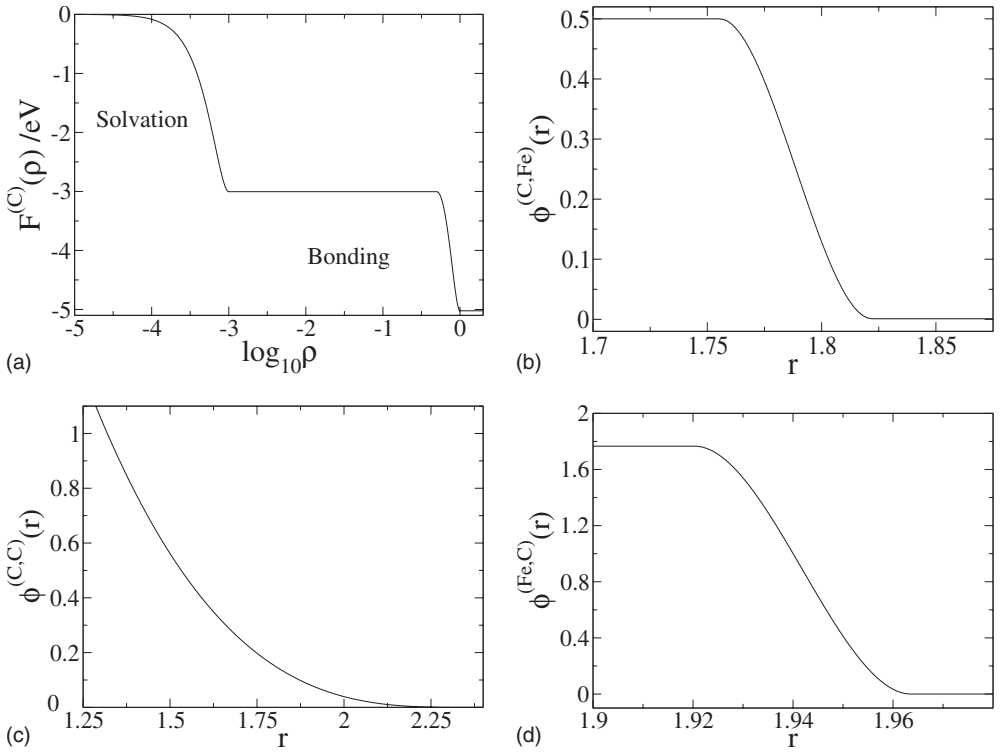

FIG. 1. Fitted forms for the embedding functions showing the implementation of solvation and bonding via the embedding parts of our potential. The regions associated with solvation and bonding within the carbon embedding function, $F^{(C)}$, are indicated. Energies are in electron volts and distances in angstroms.

carbon dissolves in iron and have been chosen to ensure that a substitutionally sited carbon is in solution. The radii, r_1 and r_2, set the range of covalent bond formation and have been empirically fitted here.

We implement carbon-carbon bonding through $\phi^{(C,C)}$. A simple-cubic form with cutoff was found to be sufficient,

$$\phi^{(C,C)}(r) = a(r_c - r)^3 H(r_c - r), \tag{7}$$

where H is the Heaviside step function. The coefficient, a, and cutoff, r_c, were empirically fitted here.

Overall the above forms ensure that $F^{(C)}$ initially saturates upon solvation of carbon and further saturates, following the Tersoff and Brenner style,[13–15] when carbon bonds to two near-neighbor irons (through $\phi^{(C,Fe)}$) or one near-neighbor carbon atom (through $\phi^{(C,C)}$).

Finally, we model the effect of carbon on nearby iron atoms, through $\phi^{(Fe,C)}$, as additional broadening of the iron d band due to hybridization with the carbon s and p states. We take the following saturating form,

$$\phi^{(Fe,C)}(r) = \begin{cases} \phi_{sat} & r \le r_1 \\ \phi_1^{(Fe,C)}(r) & r_1 < r \le r_2 \\ 0 & r > r_2 \end{cases}, \tag{8}$$

where the cubic interpolating polynomial, $\phi_1^{(C,Fe)}$, is chosen to ensure continuity down to the first derivative. We initially fitted with standard forms such as splines but they were found to be less effective at modeling the data. The saturation value, ϕ_{sat}, and the two radii were fitted empirically here.

The resulting forms for the embedding parts of the potential are shown in Fig. 1.

III. FITTING STRATEGY

To parametrize our potential we used *ab initio* data[21] describing the energetics and local geometries of carbon in pure α iron, and the binding of carbon to vacancy and $\langle 110 \rangle$-self-interstitial type crystal defects. This data is consistent with experiment, including the binding of one and/or two carbons to a vacancy, as a rate theory analysis[28] of positron lifetime measurements[29] has shown. For self-consistency and on account of its wider database, we fit to DFT throughout except for the solvation energy for atomic carbon in α iron of 6.27 eV which was inferred from experiment:[30] DFT is known to give a poor description of the free atom.

We initially fitted to data from configurations where carbon-carbon interactions do not play a part, similar to the strategy used by Lau *et al.*[25] This allowed us to determine the iron-carbon interaction parts of the potential first before proceeding to determine the carbon-carbon interactions using the remaining data.

Constant volume relaxation was used within the fitting procedure for consistency with the *ab initio* data and to favor accurate energy reproduction (at 0 K) over that of configuration geometry. Occasionally, this relaxation algorithm failed to find the global energy minimum for a configuration during the fit. This was especially true of those configurations containing interacting $\langle 110 \rangle$-self-interstitial defects and

TABLE I. Fitted parameters for the pair potential, $V^{(\mathrm{Fe,C})}$. Energies are in electron volts and lengths in angstroms.

	$V^{(\mathrm{Fe,C})}$	
i	s_i	f_i
0	0.92	
1	1.7286	1.4445301451182067
2	1.88	−0.11197619824300484
3	2.25	−0.03712159216974577
4	2.42	−0.24932947183918894
5	2.7244	0.05596022455557193
6	3.1581	−0.1716858029483243
7	3.5	

carbon. The problem was resolved by including the true global minima as restart points for the relaxation algorithm and refitting.

The final fitted parameters for our iron-carbon potential are given in Tables I–III. The polynomial interpolation functions defined earlier for the potential functions can be determined directly from these parameters.

IV. RESULTS AND DISCUSSION

In Table IV we compare the present potential with examples of pair (Johnson),[22] Finnis-Sinclair (Lau),[25] and conventional EAM potentials (Raulot).[31] Our own attempts to parametrize these forms of potential gave similar results. We concentrate on configurations which are important in MD and kMC, either as bound states or migration barriers.

We define the binding energy of n defects and impurities, $\{A_i\}$, to be

$$E_b(\{A_i\}) = \left[\sum_{i=1}^{n} E(A_i)\right] - [E(\{A_i\}) + (n-1)E_0], \qquad (9)$$

where $E(A_i)$ is the energy for a configuration containing A_i only, $E(\{A_i\})$ refers to a configuration containing all the interacting entities, and E_0 refers to a configuration containing no defects or impurities, i.e., bulk α iron.

All potentials reproduce the relaxed *ab initio* geometries around octahedrally and tetrahedrally sited carbon accurately, and correctly fit the octahedral site as the more stable of these two. The solvation energy was not fitted by Johnson or Raulot, leading to an error of several electron volts. This can be interpreted as an error in describing free carbon atoms, and so is not serious unless one is interested in deposition or sputtering. The dynamics of carbon in α iron is governed by the migration barrier energy. Resistivity recovery measurements yield a barrier height of 0.88 eV,[32] in good agreement with *ab initio* values[21,25] of 0.90 eV and 0.86 eV. Only the Lau potential fails here, causing carbon to diffuse some five orders of magnitude too fast at room temperature and faster than vacancies. An MD simulation at 1400 K of a 2000 atom bcc iron lattice containing a single carbon atom showed that carbon migrates exclusively from octahedral to adjacent octahedral site via a tetrahedral intermediary with our potential.

Positive carbon-carbon binding is not observed in the *ab initio* calculations for nearby octahedral sites in α iron and only the Johnson potential stabilizes carbon there. At longer range carbons can interact via strain fields, an effect which gives rise to tetragonal martensite. Correct coupling to strain fields is important for modeling Cottrell atmospheres around dislocations, the atomistic explanation for the strength of steel.[33] All the potentials correctly show this effect.

The interaction of carbon with vacancies is relevant for creep resistance and radiation damage. *Ab initio* calculations show that at low temperature vacancies bind to a single carbon by about 0.5 eV. A second carbon can also bind to the vacancy either opposite or preferably adjacent to the first with an additional 1 eV of binding. Previous potentials fail to capture this effect, either by overestimating the binding of a single carbon (Lau), the absence of positive carbon-carbon interactions (Johnson), or both (Raulot). In these models carbon binds more strongly to a second vacancy than one already containing a single carbon. Our potential, in contrast, describes this situation well by avoiding excessive carbon-vacancy binding and by including covalent carbon-carbon bonding. In order to investigate the dynamics of carbon in the presence of a vacancy defect at a qualitative level, we performed an MD simulation under the same conditions as specified previously for carbon in bcc iron but now with a

TABLE II. Fitted parameters for the pair potential, $V^{(\mathrm{C,C})}$. Energies are in electron volts and lengths in angstroms.

	$V^{(\mathrm{C,C})}$	
i	s_i	f_i
0	1.0	
1	1.2857838598417968	7.506546603651753
2	1.8008513964923578	0.9366343321217112
3	2.2863452818753887	0.4256080873202003
4	3.5	

TABLE III. Fitted parameters for the embedding parts of the iron-carbon potential. Energies are in electron volts and lengths are in angstroms.

	E_{sol}	E_{bond}
$F^{(\mathrm{C})}$	−3.0046321427471687	−2.0181254292659294
$\phi^{(\mathrm{C,Fe})}$	r_1	r_2
	1.7554340024999981	1.8220492635
	r_3	r_4
	2.5	3.5
$\phi^{(\mathrm{Fe,C})}$	r_1	r_2
	1.9203	1.9635780468749997
	ϕ_{sat}	
	1.766097265625	
$\phi^{(\mathrm{C,C})}$	a	r_c
	0.9130368825588165	2.350400993501056

TABLE IV. Comparison of our potential and those of Raulot (Ref. 31), Lau (Ref. 25), and Johnson (Ref. 22) with *ab initio* energy data (Ref. 21). The solvation energy, E_s, has been inferred from Ref. 30. The migration energy for carbon, E_m, is the energy difference between tetrahedrally and octahedrally sited carbon [see Fig. 2(a)]. All other reported values are binding energies as defined in Eq. (9) between an octahedrally sited carbon (C) and a second carbon (C), vacancy (V), or SI defect or between two carbons and a vacancy. When two binding entities are present, the configuration is identified by the notation introduced in Figs. 2(b) and 3, and additionally by their separation vector in lattice units before relaxation. For carbon-carbon-vacancy binding the carbons are either on opposite sides of the vacancy [e.g., at $(0,0,\frac{1}{2})$ and $(0,0,-\frac{1}{2})$] or adjacent to one another [e.g., at $(\frac{1}{2},0,0)$ and $(0,0,\frac{1}{2})$].

Energies [eV]	*Ab initio*	This work	Raulot	Lau	Johnson
E_s	+6.27	+6.27	+10.05	+7.15	+1.32
E_m	+0.90	+0.89	+0.85	+0.63	+0.86
E_b(C,C)					
2:$(\frac{1}{2},\frac{1}{2},\frac{1}{2})$	−0.09	−0.07	−0.17	−0.19	+0.12
7:(1,1,1)	+0.16	+0.05	+0.03	+0.01	+0.04
E_b(C,V)					
1:$(0,0,\frac{1}{2})$	+0.47	+0.49	+0.83	+0.76	+0.41
2:$(\frac{1}{2},\frac{1}{2},0)$	−0.01	−0.08	+0.01	−0.11	−0.42
4:$(\frac{1}{2},\frac{1}{2},1)$		+0.17	+0.17	+0.24	+0.15
E_b(C,C,V)					
Adjacent	+1.50	+1.38	+0.52	+1.39	+0.83
Opposite	+1.07	+0.65	+1.13	+0.94	+0.82
E_b(C,SI)					
1a:$(0,0,\frac{1}{2})$	−0.19	−0.14	+0.37	+0.68	+0.55
2a:$(0,\frac{1}{2},\frac{1}{2})$	−0.09	−0.04	+0.23	+0.20	+0.24
2c:$(-\frac{1}{2},\frac{1}{2},0)$	−0.31	−0.29	+0.07	+0.12	+0.10
5a:$(1,1,\frac{1}{2})$	+0.09	+0.20	+0.19	+0.08	+0.22
6a:$(0,0,\frac{3}{2})$		+0.20	+0.12	+0.21	+0.13

vacancy present. The simulation showed that carbon acts as a trap for the faster moving vacancies and that escape is possible by making successive jumps in ⟨111⟩ directions. The first escape jump was exclusively from $(0,0,\frac{1}{2})$ to $(\frac{1}{2},\frac{1}{2},1)$, i.e., no instance of the alternative jump to $(\frac{1}{2},\frac{1}{2},0)$. Energetically this is the preferred jump, as can be seen from the binding energies. The $(\frac{1}{2},\frac{1}{2},1)$ site in fact shows positive binding for all potentials, a result that is currently not verified by *ab initio* but seems likely. From this site the most likely jump was a return to $(0,0,\frac{1}{2})$ but successive jumps away from the carbon did occasionally result in escape for the vacancy.

Iron self-interstitials are typically only important in irradiated samples. However, they represent the simplest model

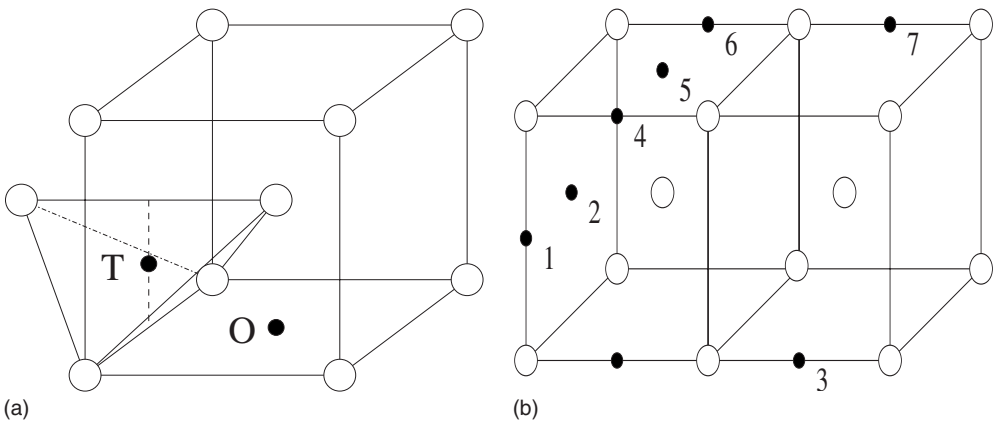

FIG. 2. (a) O and T interstitial sites for carbon (black circles) in an unrelaxed bcc unit cell of iron atoms (white circles). (b) Configurations containing two interacting carbon atoms in neighboring octahedral sites. Distinct configurations are labeled by the position of the second carbon atom.

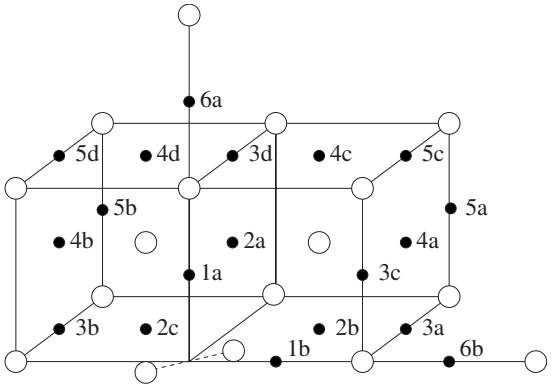

FIG. 3. Distinct octahedral sites for carbon surrounding a ⟨110⟩-self-interstitial defect. The site nomenclature is also valid for a vacancy defect after removing the superfluous letter.

for the binding of carbon to overcoordinated defects such as those present in grain boundaries and dislocations, and so represent an important test of potential transferability. The *ab initio* data shows a strong repulsion between overcoordinated defects and nearby carbon atoms. By contrast previous potentials all show strong binding. Despite significant effort, we were unable to refit these potentials to reproduce this repulsion in addition to the other targets from our fitting database. Thus we conclude it is the functional form of these potentials, not the parametrization, which gives the binding. Our covalent-style potential has saturation of the carbon embedding function, which means that any extra nearby iron atoms do not give increased binding. Thus we were able to successfully fit the carbon-⟨110⟩-self-interstitial (SI) energies by better describing the physics involved.

All potentials and the *ab initio* data show positive binding between interstitials and carbon at separations where strain field effects are expected to dominate. This is consistent with experiment[29,32] which shows a similar binding of 0.1 eV between carbon and a highly mobile point defect, and corroborates their interpretation that this defect is a self-interstitial.

V. CONCLUSIONS

In conclusion, we used electronic structure to devise heuristics for building an interatomic force model for iron-carbon. The model incorporates the magnetic second-moment tight-binding picture for iron, charge transfer from iron to carbon, and a covalent picture of localized *p* bonding around carbon atoms. The potential is suitable for large scale MD, being short-ranged and computationally equivalent to EAM. The formalism allows us to correctly predict the interactions between carbon and a range of defects in iron, many of which are intractable with conventional potentials. This gives us good confidence in its transferability to different environments in ferritic steels.

ACKNOWLEDGMENTS

We gratefully acknowledge support from EU PERFECT and GETMAT programs, and EPSRC Grant No. GR/S81186.

*dhepburn@ph.ed.ac.uk
†gjackland@ed.ac.uk

[1] C. C. Fu, D. T. Torre, F. Willaime, J. L. Bocquet, and A. Barbu, Nat. Mater. **4**, 68 (2005).
[2] C. Domain and G. Monnet, Phys. Rev. Lett. **95**, 215506 (2005).
[3] D. J. Bacon, F. Gao, and Y. N. Osetsky, J. Nucl. Mater. **276**, 1 (2000).
[4] E. Stoller, J. Nucl. Mater. **276**, 22 (2000).
[5] L. Malerba, J. Nucl. Mater. **351**, 28 (2006).
[6] G. J. Ackland, M. I. Mendelev, D. J. Srolovitz, S. Han, and A. V. Barashev, J. Phys.: Condens. Matter **16**, S2629 (2004).
[7] M. I. Mendelev, S. Han, D. J. Srolovitz, G. J. Ackland, D. Y. Sun, and M. Asta, Philos. Mag. **83**, 3977 (2003).
[8] G. J. Ackland, D. J. Bacon, A. F. Calder, and T. Harry, Philos. Mag. A **75**, 713 (1997).
[9] M. Marchese, G. Jacucci, and C. P. Flynn, Philos. Mag. Lett. **57**, 25 (1988).
[10] M. S. Daw and M. I. Baskes, Phys. Rev. B **29**, 6443 (1984).
[11] M. W. Finnis and J. E. Sinclair, Philos. Mag. A **50**, 45 (1984).
[12] G. J. Ackland and S. K. Reed, Phys. Rev. B **67**, 174108 (2003).
[13] J. Tersoff, Phys. Rev. Lett. **61**, 2879 (1988).
[14] D. W. Brenner, Phys. Rev. B **42**, 9458 (1990).
[15] G. Ackland, Phys. Rev. B **40**, 10351 (1989).
[16] F. Ducastelle, J. Phys. (Paris) **31**, 1055 (1970).
[17] F. Ducastelle and F. Cyrot-Lackmann, J. Phys. Chem. Solids **32**, 285 (1971).
[18] S. L. Dudarev and P. M. Derlet, J. Phys.: Condens. Matter **17**, 7097 (2005).
[19] G. J. Ackland, J. Nucl. Mater. **351**, 20 (2006).
[20] A. Sutton, M. W. Finnis, D. G. Pettifor, and Y. Ohta, J. Phys. C **21**, 35 (1988).
[21] C. Domain, C. S. Becquart, and J. Foct, Phys. Rev. B **69**, 144112 (2004); (private communications).
[22] R. A. Johnson, Phys. Rev. **134**, A1329 (1964); Phys. Rev. B **5**, 1642 (1972).
[23] D. E. Jiang and E. A. Carter, Phys. Rev. B **67**, 214103 (2003).
[24] C. J. Först, J. Slycke, K. J. Van Vliet, and S. Yip, Phys. Rev. Lett. **96**, 175501 (2006).
[25] T. T. Lau, C. J. Forst, X. Lin, J. D. Gale, S. Yip, and K. J. Van Vliet, Phys. Rev. Lett. **98**, 215501 (2007).
[26] C. C. Fu, E. Meslin, A. Barbu, F. Willaime, and V. Oison, Solid State Phenom. **139**, 157 (2008).
[27] J. P. Biersack and J. F. Ziegler, Nucl. Instrum. Methods **194**, 93 (1982).
[28] K. Tapasa, A. V. Barashev, D. J. Bacon, and Yu. N. Osetsky, Acta Mater. **55**, 1 (2007).
[29] A. Vehanen, P. Hautojärvi, J. Johansson, J. Yli-Kauppila, and P. Moser, Phys. Rev. B **25**, 762 (1982).
[30] E. F. Petrova, M. I. Lapshina, and L. A. Shvartsman, Metal Sci. Heat Treatment **2**, 207 (1960).
[31] C. S. Becquart, J. M. Raulot, G. Bencteux, C. Domain, M. Perez, S. Garruchet, and H. Nguyen, Comput. Mater. Sci. **40**, 119 (2007).
[32] S. Takaki, J. Fuss, H. Kugler, U. Dedek, and H. Schultz, Radiat. Eff. **79**, 87 (1983).
[33] A. Cottrell and B. Bilby, Proc. Phys. Soc., London, Sect. A **62**, 49 (1949).